




# Discovery of a bulk C36-type MgZn<sub>2</sub> structure step by step transformed from the C14 prototype laves phase structure

Tong Yang<sup>1</sup>, Jiangbo Lu<sup>2</sup>, Kai Li<sup>1,\*</sup> , Yi Kong<sup>1,\*</sup>, Zhenjun Zhang<sup>3</sup>, Qianxin Long<sup>4</sup>, Xinyue Lan<sup>1</sup>, Qiang Lu<sup>1</sup>, and Yong Du<sup>1</sup>

<sup>1</sup> State Key Laboratory of Powder Metallurgy, Central South University, Changsha 410083, China

<sup>2</sup> School of Physics and Information Technology, Shaanxi Normal University, Xi'an 710119, China

<sup>3</sup> Materials Fatigue and Fracture Division, Institute of Metal Research, Chinese Academy of Sciences, Shenyang 110016, China

<sup>4</sup> School of Materials Science and Engineering and Guangxi Key Laboratory of Information Materials, Guilin University of Electronic Technology, Guilin 541004, China

Received: 15 August 2021

Accepted: 9 November 2021

Published online:

3 January 2022

© The Author(s), under exclusive licence to Springer Science+Business Media, LLC, part of Springer Nature 2021

## ABSTRACT

MgZn<sub>2</sub> phase is the prototype of hexagonal C14 Laves phase, acting as an important intermetallic compound. Here we first observe the atomic-scale structure of C36-type MgZn<sub>2</sub> Laves phase by high-angle annular dark-field scanning transmission electron microscopy. Solid atomic-scale evidence is provided for the finding that C14 structural precipitate can totally transform to C36 structure during extremely long-time over-aging at medium temperatures in an Al-Zn-Mg alloy, rather than C36 stacking faults as previously reported. Intermediate structures between C14 and C36 were observed along [0001] and  $[\bar{1} 2 \bar{1} 0]$  directions. Two possible transformation paths are illustrated based on the synchroshear mechanism, and their atomic resolution evidence is provided. Ab initio molecular dynamics calculations support our inference on the transformation process. This type of Laves phase transformation provides a new strategy for designing alloys that contain Laves phases as hardening precipitates.

## Introduction

Laves phases, with the topologically close-packed (TCP) structure, constitute the largest single class of intermetallics with a chemical formula of AB<sub>2</sub> [1].

From the viewpoint of crystal structure, only three types of Laves phase have been observed, including C14 structure (prototype: MgZn<sub>2</sub>, hexagonal, space group: P63/mmc, stacking sequence: ...ABAB...), C15 structure (prototype: MgCu<sub>2</sub>, cubic, space group:

Handling Editor: Megumi Kawasaki.

Address correspondence to E-mail: leking@csu.edu.cn; yikong@csu.edu.cn

<https://doi.org/10.1007/s10853-021-06711-6>

Fd  $\bar{3}m$ , stacking sequence: ...ABCABC...), and C36 structure (prototype: MgNi<sub>2</sub>, hexagonal, space group: P63/mmc, stacking sequence: ...ABACABAC...) [2–4]. The mutual structure transformation between Laves phases is possible when the material undergoes certain thermal processes and/or mechanical deformations [5, 6]. For instance, the partial transformation of C14 structure to other Laves structures has been widely reported in former investigations [7–10]. Such structures are commonly defined as stacking faults because of the shearing nature of the structural changes among different Laves structures.

The C15 and C14 phases are, respectively, the second and fifth most frequent structural types of intermetallic compound, whereas the C36-type phase is far less abundant [11]. Previous studies reported the C36 structure as characteristic only for some Laves phase compounds and were assumed as an intermediate state between C14 and C15 [12]. This is consistent with our recent findings that part of C36 structures can occur as stacking faults in C14 MgZn<sub>2</sub> precipitates in an over-aged Al-Zn-Mg alloy [13]. So far, it is not clear whether the C36-type MgZn<sub>2</sub> can exist as a bulk phase or a bulk precipitate (rather than defects in precipitates). Moreover, straightforwardly interpretable atomic-scale observations of the C36 Laves phase have not been provided.

On the other hand, previous investigations revealed that Laves phase has good strengthening properties due to the close-packed structure; thus, their precipitation is desired in high-strength materials [14–17]. In Al-Zn-Mg alloys, the typical C14-MgZn<sub>2</sub> phase, designated as  $\eta$ , is an important hardening precipitate in an over-aged state and thus has been widely investigated [18–20]. Moreover, C14-type MgZn<sub>2</sub> is also the major strengthening phase in Mg-Zn alloys, named as  $\beta'_1$  phase, which also receives much attention in Mg-based alloy [21]. However, as for the comparison between effects of different type Laves phase crystal structures on mechanical properties, researchers mainly pay attention to the comparison between C15 and C14 types because hexagonal C14-type and C36-type are hard to distinguish in previously used methods like X-ray diffraction (XRD) or high-resolution transmission electron microscopy (HRTEM). For example, Rabadia et al. [22] found that the C15-type Laves phase as reinforcement in titanium alloys deformed more smoothly than the C14-type Laves phase. In

their work, the former exhibited a better dislocation pinning ability than the latter, but they did not compare the C36-type phase with C14. Tan et al. [23] investigated the mechanical properties of Fe<sub>2</sub>Zr Laves reinforcement phase in Fe-Cr-Zr alloys, but they cannot identify the hexagonal structure as either C36 or C14 due to the difficult differentiation from XRD patterns. In addition, no previous investigation found the phase transformation between C14-type and C36-type precipitates. As a result, the correlation between mechanical properties and precipitate behaviors in corresponding alloys cannot be conducted. Atomic-scale observations of these important intermetallics in Laves phase precipitates are necessary for finding how the mechanical properties are affected. Meanwhile, according to the general perception of the Laves phase prototypes, it would be very interesting to investigate the less frequently studied C36-MgZn<sub>2</sub> Laves phase, for the purpose to update the understanding of different strengthening Laves phases in wide-spread compounds.

In this work, the atomic-scale transformation of MgZn<sub>2</sub> Laves phase precipitates from C14 to C36 structures during the process of long-time aging is firstly reported. High-angle annular dark-field scanning transmission electron microscopy (HAADF-STEM) at low damage conditions was used to observe structures of precipitated Laves phases in an industrial Al-Zn-Mg alloy. The possible intermediate paths (step by step) from C14 to C36 structure were analyzed, based on experimental microscopy results explained with the aid of *Ab initio* molecular dynamics (AIMD) calculations. These new fundamental understandings on phase transition of prototype Laves phases may provide guidance for future research on the relation between the Laves phase precipitates and mechanical performance of materials.

## Material and methods

### Materials preparation

In this work, a commercial 7B05 Al alloy with 4.31% Zn, 1.41% Mg, 0.31% Mn, 0.14% Fe, and 0.12% Cu (in wt.%) was used. The alloy was at an over-aged state for 568 h at 120 °C by T5 treatment. Then, the aging was prolonged for 20 more days to reach a total aging time of 1048 h at 120 °C (T5 + 20 d state) in order to

observe the consequential phase transformation. Square plates of 20 mm × 20 mm × 1 mm were cut from these overaged alloys. These plates were firstly ground to slices as thin as 40–80 μm and then several disks with a diameter of 3 mm were punched from each slice. The specimens were electropolished into foils by using a mixture of 70 vol.% methanol and 30 vol.% nitric acid as electrolyte, at the polishing temperature of −30 °C and the voltage of 16 V in a Struers Tenupol-5 twin-jet electropolisher.

### Microstructure characterization

Atomic-resolution high-angle annular dark-field scanning transmission electron microscopy (HAADF-STEM) was carried out on a Thermo Fisher Titan Cubed Themis G2 300 TEM equipped with a probe Cs-corrector operated at the verified low-damage voltage of 80 kV. The convergence angle used to record the HAADF-STEM images was 25.6 mrad, and the inner and outer collection angles were 63 and 200 mrad, respectively. Each HAADF-STEM image shown in this work was acquired by superimposing 50–100 fast scan images recorded with the drift-corrected frame integration (DCFI) technology [24]. This technology can apparently reduce noise and image deformations due to the integration of more intensity over a longer time and a more rapid scan for each frame compared to conventional single scan technology. This microscope is also equipped with a Super-X detector to provide atomic resolution in EDX elemental mapping.

### Ab initio molecular dynamics calculation

The total energies of C14 and C36 structure under the aging temperature (393 K) were calculated by Ab initio molecular dynamics (AIMD) within the framework of density functional theory (DFT) [25, 26]. The AIMD time step was 1.0 fs, and the total simulation time of each simulation was 4000 fs. A convergence criterion of 1 meV (per simulation box) for ionic and 0.1 meV for electronic loops, energy cut off of 400 eV, and a single point (Gamma) k-mesh were used. Considering the aging temperatures, the Nosé–Hoover thermostat were used to set the temperature within a canonical NVT ensemble [27]. Supercells of C14 (2 × 2 × 4) and C36 (2 × 2 × 2) were created with 192 atoms in order to calculate accurately (cif structures for calculation are added in

the Supplementary Material). Therefore, by combining experimental results with AIMD calculations, the complete bulk phase transformation from C14 to C36 was found and the possible intermediate paths (step by step) were analyzed.

## Results and discussion

### The observed bulk C36 structure of the MgZn<sub>2</sub> precipitate

Figure 1 shows the phase transformation by exhibiting the hexagonal stacking configurations of MgZn<sub>2</sub> phases with C14-type and C36-type structures at different aging times. The orientation relationship (OR) between these two η precipitates and the Al matrix is as follows:  $(\bar{1} 2 \bar{1} 0)_\eta // (1 \bar{1} \bar{1})_{Al}$ ;  $[0001]_\eta // [110]_{Al}$ , classified as η<sub>4</sub> [20] (the Fast Fourier Transform patterns of these two images are the same, as displayed in Supplementary Document Fig. S1). As is reported before, HAADF-STEM images provide atomic number (Z) contrast (among atomic columns) proportional to  $Z^{1.7-1.9}$  [30]. C14 structure is made up of hexagonal units (measured as  $a = 5.24 \pm 0.26$  nm, marked by red borders) with 6 Mg columns in the border and 7 Zn columns in the center in Fig. 1b, c. The central Zn column in the unit has double Zn atom numbers compared with the other six Zn columns, and thus, it shows the brightest intensity in the HAADF-STEM image. There is a sharp contrast between the heavier Zn ( $Z_{Zn} = 30$ ) columns and lighter Mg ( $Z_{Mg} = 12$ ) columns, and the other 6 Mg columns show very weak intensity [30]. Similarly, the C36 structure in Fig. 1e is also made up of hexagonal units (measured as  $a = 5.16 \pm 0.19$  nm). However, its internal structure is quite different from that of C14-MgZn<sub>2</sub>. The pure Mg atomic columns at the six corners of the red hexagonal unit of the C14 structure are showing the weakest contrast (see Fig. 1c), but in the C36 structure, these columns at the corners show the brightest intensity as they contain 50% Mg and 50% Zn atoms (refer to the crystal model of C36 in Fig. 1h and the Supplementary cif files). In the meantime, the brightest Zn column in the unit center of C14 has turned into the darkest Mg column in C36. The comparison between their cell parameters is listed in Table 1. EDX mappings are also conducted for this C36 precipitate to further confirm the elements segregation inside are Mg and Zn, but the precipitate is

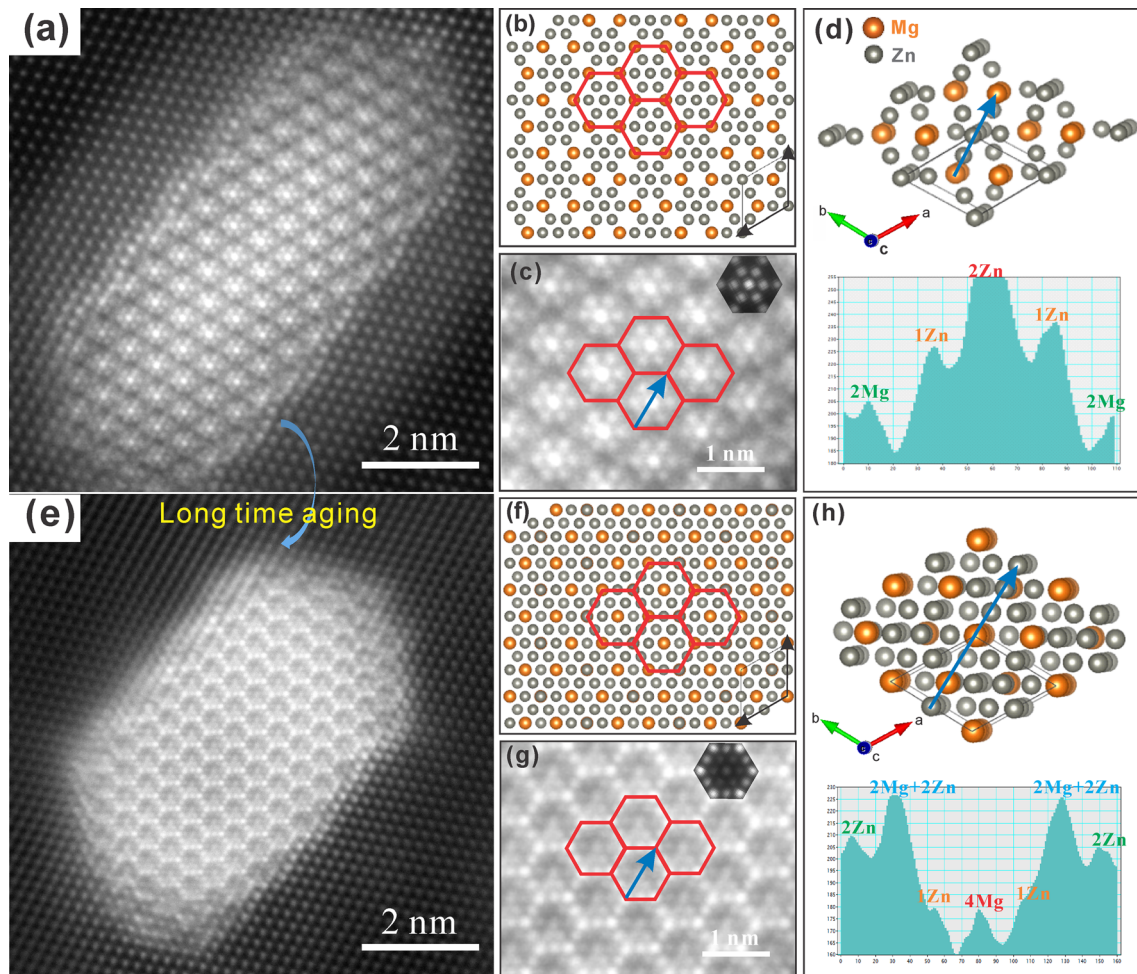


**Figure 1** Comparison between C14 and C36 atomic-scale structures of  $\text{MgZn}_2$  precipitates in 7B05 alloy, both viewed from  $[0001]_{\eta} // [110]_{\text{Al}}$  zone axis. **a** HAADF-STEM image of C14- $\text{MgZn}_2$  structure (T5 state). **b** The corresponding crystal structure model of C14- $\text{MgZn}_2$  determined by Komura et al. [28]. **c** An enlarged area in (a). **d** The image of intensity line profiles among atom columns in (c) in comparison with C14 structure

model. **e** HAADF-STEM image of C36- $\text{MgZn}_2$  structure (T5 + 20 d state). **f** The corresponding crystal structure model of C36- $\text{MgZn}_2$  modified from that of  $\text{MgNi}_2$  [28]. **g** An enlarged area in (e). **h** The image intensity line profiles among atom columns in (g) in comparison with C36 structure model. The simulated HAADF-STEM images by QSTEM [29] were inserted in (c) and (g).

vulnerable to electron beam as shown in Supplementary Document Fig. S2. Other similar HAADF-STEM images of precipitate with C36 structure are displayed in Supplementary Document Fig. S3, to prove that the phase transformation in bulk precipitates is not an accidental phenomenon. All in all, the transformation from C14 to C36 will totally change

the atom arrangement, but the orientation and the morphology have little variation. Such a difference can hardly be noticed by conventional HRTEM characterizations in this zone axis [31, 32].

**Table 1** Structure parameters of C14 and C36  $\text{MgZn}_2$

| $\text{MgZn}_2$           | $a/\text{nm}$ (C14) | $a/\text{nm}$ (C36) | $c/\text{nm}$ (C14) | $c/\text{nm}$ (C36) |
|---------------------------|---------------------|---------------------|---------------------|---------------------|
| Initial established model | 5.22                | 5.22                | 8.57                | 17.14               |
| Relaxed model in AIMD     | 5.32                | 5.29                | 8.16                | 16.52               |
| Measured in STEM image    | $5.24 \pm 0.26$     | $5.16 \pm 0.19$     | /                   | /                   |

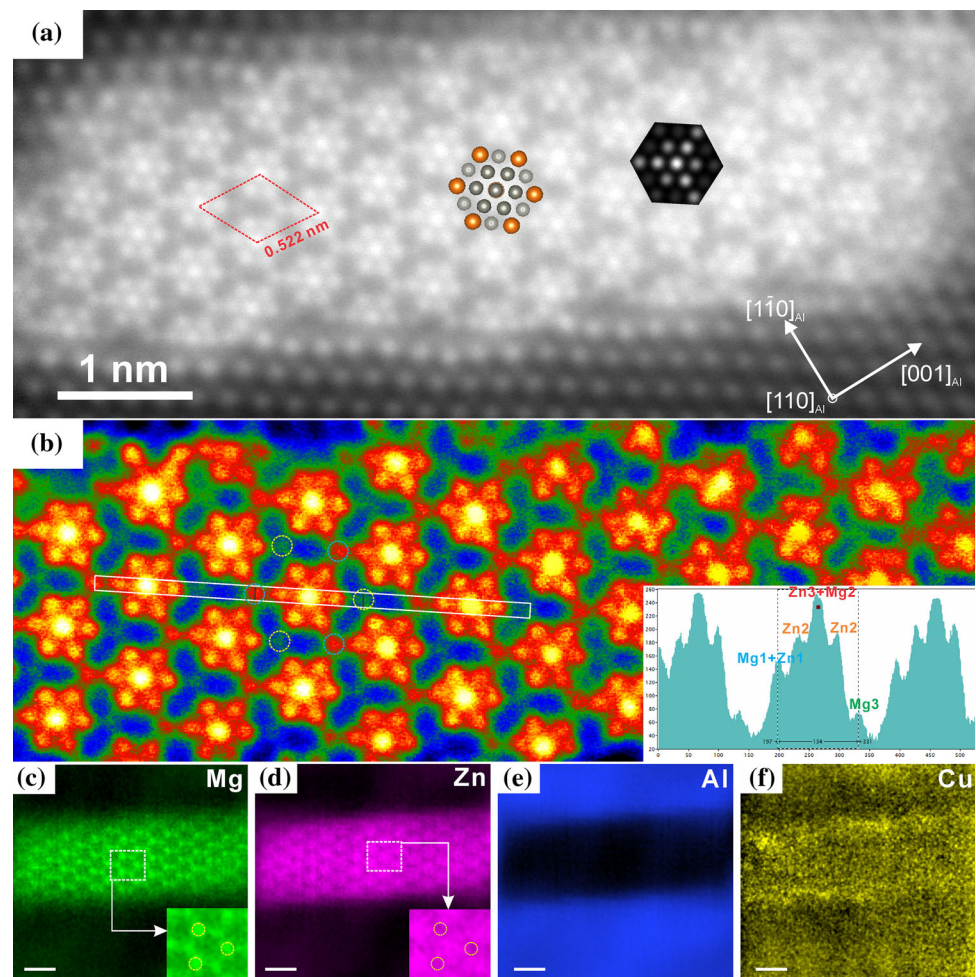


## The step-by-step transformation of MgZn<sub>2</sub> precipitates viewed from [0001]

Figure 2a shows the atomic-resolution HAADF-STEM images of  $\eta$  precipitates with stacking behaviors between C14 and C36 structures. The OR of this precipitate and Al matrix is as same as that in Fig. 1a. However, the atom columns intensity cannot match that of C14 structure in Fig. 1a, especially on the 6 Mg columns at the hexagonal corners. It is obvious that 3 Mg columns have a higher intensity than the other 3 Mg columns as shown in Fig. 2b after removing the background. Atomic-scale EDX mapping images in Fig. 2c–f show solute enrichment in all atomic columns. Firstly, there is almost no Al enrichment inside this precipitate, as it appears dark in Fig. 2e. Secondly, due to the extremely low Cu content of this alloy, the distribution of Cu element shown in Fig. 2f is with a much more noisy background than of other elements, except for the fact that

only a few Cu atoms segregate at the MgZn<sub>2</sub> / Al interface. This is similar to the EDX mapping in C36 structure as shown in Fig. S2. The segregation of Cu atoms at precipitate/matrix interface is not a rare phenomenon in Al alloys [33], and therefore, it will not be discussed here. As for the enrichment of Mg and Zn atoms, it is obvious that the darker atomic columns as indicated in yellow circles in Fig. 2b are with higher Mg concentration than the other 3 columns as displayed in Fig. 2c, meanwhile, with very little Zn concentration as revealed in Fig. 2d. Therefore, these columns can be inferred as nearly pure Mg columns. In contrast, the brighter columns in HAADF-STEM images are with less but still noticeable Mg concentration compared to columns, and they contain a substantial amount of Zn as shown in Fig. 2d. They can be explained as columns mixed with both Mg and Zn atoms. Such mixing can only be found in a periodic C14 structure containing 2R stacking layers inserted among R layers (R means

**Figure 2** HAADF-STEM image and EDX mapping images of precipitate with stacked structure in-between C14 and C36 structures. **a** an  $\eta$  precipitate (T5 state) viewed along  $[0001]_{\eta}$ . The C14 model with one 2R stacking fault inserted as well as the corresponding simulated HAADF-STEM image are inserted. **b** HAADF-STEM image of the precipitate with background removed (see details in Supplementary Data) and pseudocolor. The intensity map inserted is obtained along the white bar. **c–f** are atomic-resolution EDX mappings of Mg, Zn, Al, Cu elements, respectively, and the scale bars are 1 nm.



rhombohedral Zn units along  $[\bar{1} 2 \bar{1} 0]$  by researchers [9] as shown in the model of Fig. 6). The correspondingly simulated HAADF-STEM image by QSTEM script [28] in Fig. 2a can well fit the experimental image contrast. More analyses are illustrated in Fig. 3 to verify the effect of stacking faults on atoms columns' contrast viewed along  $[0001]$ .

The schematic diagrams of the initial transformation step are displayed in Fig. 3 to explain why the HAADF-STEM images contrast of Mg atoms columns in Fig. 2a are inconsistent with the perfect C14 structure in Fig. 1a. As shown in Fig. 3b, when one 2R stacking fault is inserted into a perfect C14 structure, some Zn atoms will mix into Mg columns (see the blue circles); on the contrary, some Mg atoms will enter the middle Zn atom column (see the red circles) in the unit cell. Then, the hexagonal corners in the unit cell will show two kinds of intensity due to the different enrichment of Mg atoms. The precipitate in Fig. 2a is referred to as a C14 structure with stacking faults (2R structure), as an initial structure in the transformation process from C14 to C36. However, the number of stacking faults cannot be obtained as the view direction is  $[0001]_{\eta}$ . Therefore, more images from another view direction  $[\bar{1} 2 \bar{1} 0]_{\eta}$  are obtained in the following study to verify the transformation steps.

### The step-by-step transformation of $MgZn_2$ precipitates viewed from $[\bar{1} 2 \bar{1} 0]$

Figure 4 shows an atomic-resolution Z-contrast image of a nano-sized  $\eta$  precipitate viewed along  $[\bar{1} 2 \bar{1} 0]_{\eta}$  with a typical lath morphology on grain boundary. The OR in Fig. 4a is  $[\bar{1} 2 \bar{1} 0]_{\eta} // [1 \bar{1} 2]_{Al}$ ;  $(0001)_{\eta} // (110)_{Al}$ , corresponding to  $\eta_{11}$  [34]. It can be clearly seen that the arrangement of atoms in this precipitate is not periodic, and a large number of stacking fault structures and two irregular bands of planar defects (see the orange frames) throughout the precipitates can be observed. According to our previous study [13], the planar defects in precipitates are mainly caused by the large strain surrounding the precipitates. In this precipitate, although there is no perfect periodic C14 or C36 stacking structure, one periodic stacking with the structural units (named as  $2R + \bar{R}$ ) enlarged in Fig. 4b) has repeated 9 times as shown in the middle of Fig. 4a marked by red borders. This is the side-view evidence of the existence of  $2R + \bar{R}$  stacking behaviors in the lath-like precipitate, complementary to the end-on view image (along  $[0001]_{\eta}$ ) as shown in Fig. 2a. Meanwhile, another kind of stacking (named as  $3R + \bar{R}$ ) also appears at both ends of this precipitate, as marked in yellow dashed frames and enlarged in Fig. 4c.

It is confirmed perfect C14-MgZn<sub>2</sub> structure has a stacking sequence displayed as  $R + \bar{R}$  (zig-zag structures). In Fig. 5, two particles with a pair of

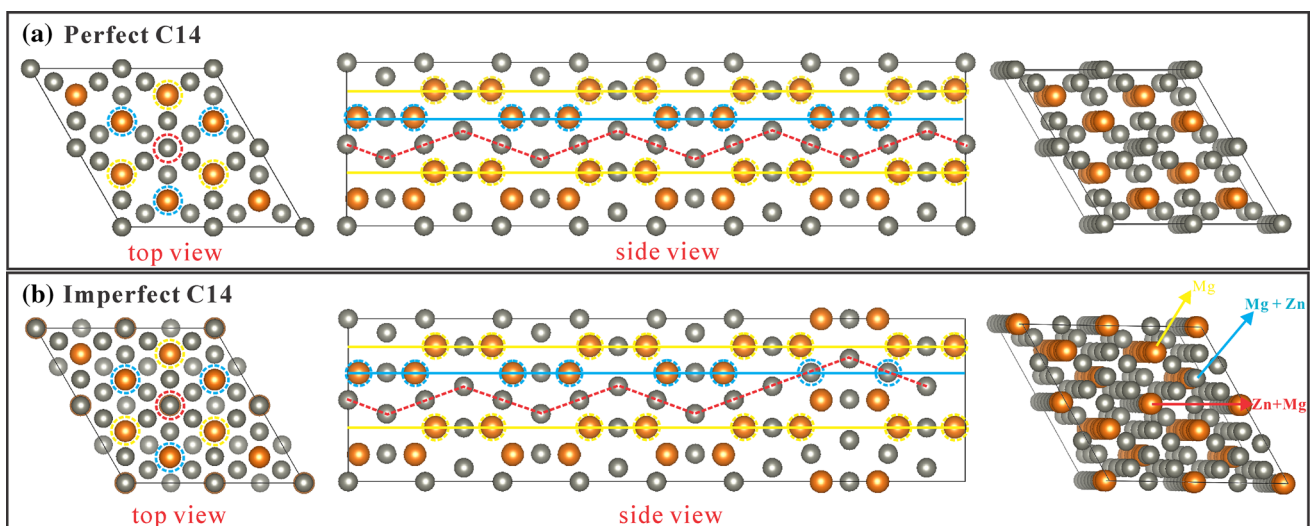
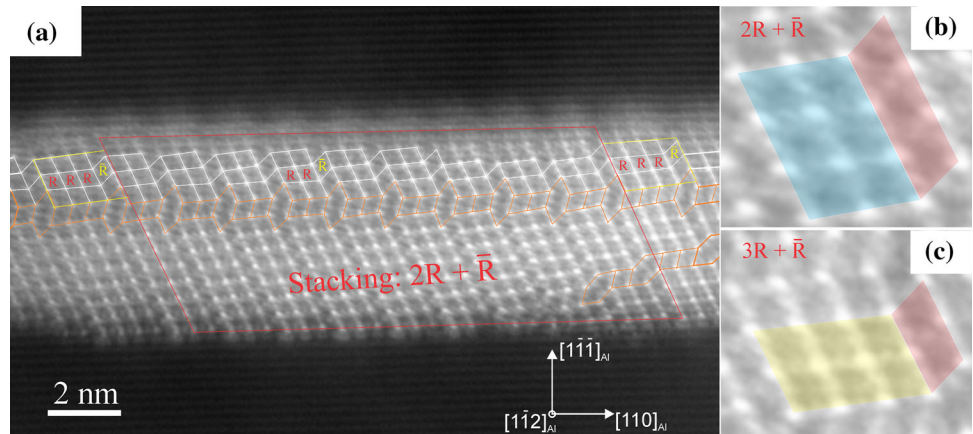


**Figure 3** Schematic diagram of the initial step of the transformation of  $MgZn_2$  phase from C14 to C36 structure. **a** Crystal model of perfect C14 structure. **b** Crystal model of an initial transformed structure inserted one 2R stacking fault.



**Figure 4** HAADF-STEM images of another precipitate with stacked structure in-between C14 and C36 structures. **a** an  $\eta$  precipitate viewed along  $[\bar{1} 2 \bar{1} 0]_{\eta}$  with complex stacked structure in-between C14 and C36 structures (T5 + 20 d state). **b, c** are enlarged areas of different stacking behaviors existing in (a).



reversed stacking faults, namely  $2R + 2 \bar{R}$ , are also observed, which correspond well with the C36 stacking sequences. These verify our inference on transformation steps. After emitting one stacking fault on a layer plane,  $3R + \bar{R}$  or  $2R + \bar{R}$  structures can be formed as detailed illustrated in Fig. 4. The atomic stacking structures are highlighted in white lines in Fig. 5, with reversed but separate  $2R$  and  $2 \bar{R}$  stacking faults, believed as one precursor of the bulk structure with complete  $2R + 2 \bar{R}$  periodicity (C36 structure). Ultimately, a total C36 structure with periodic  $2R + 2 \bar{R}$  stacking behaviors will be formed since our theoretical calculations support these inferences (see “Predicted energies of C14 and C36 structures” section). Therefore, the summary of the transformation path from C14 to C36 Laves structures of the  $MgZn_2$  precipitate during over-aging is as follows:  $R + \bar{R}$  (C14)  $\rightarrow 2R + \bar{R} / 3R + \bar{R} \rightarrow 2R + 2 \bar{R}$  (C36). More detailed schematic illustration is below.

**Schematic illustration of transformation mechanism**

By analyzing all the observations above, the step-by-step phase transformation can be explained as illustrated in Fig. 6. Due to the difference of stacking periodicities along the  $c$  axis, the  $c$  parameter of the C36 structure is twice that of the C14 structure. According to the description of Chisholm et. al. [35], the structure of all binary Laves phases consists of alternating layers of a single  $s$  layer (Zn layer in  $MgZn_2$ ) and a triple-layer stack (Mg-Zn-Mg) in two forms, designated as  $t$  and  $t'$ , which are mirror-symmetric to each other about the layer plane  $(0001)_{\eta}$  as shown in Fig. 6a, b. In C14 structure, the stacking sequence is illustrated as  $\dots s t s t' \dots$  while the stacking sequence of C36 is  $\dots s t s t s t' s t' \dots$ , which is period-doubled compared to C14 as shown in Fig. 6a, b. A most likely mechanism of phase transformation from bulk C14 to C36 is depicted in Fig. 6c. The dashed rectangles in Fig. 6c present partial

**Figure 5** HAADF-STEM images of precipitates with  $2R + 2 \bar{R}$  (C36 stacking sequence) structures, viewed along  $[\bar{1} 2 \bar{1} 0]_{\eta}$  in the over-aged (T5 + 20 d state) alloy.

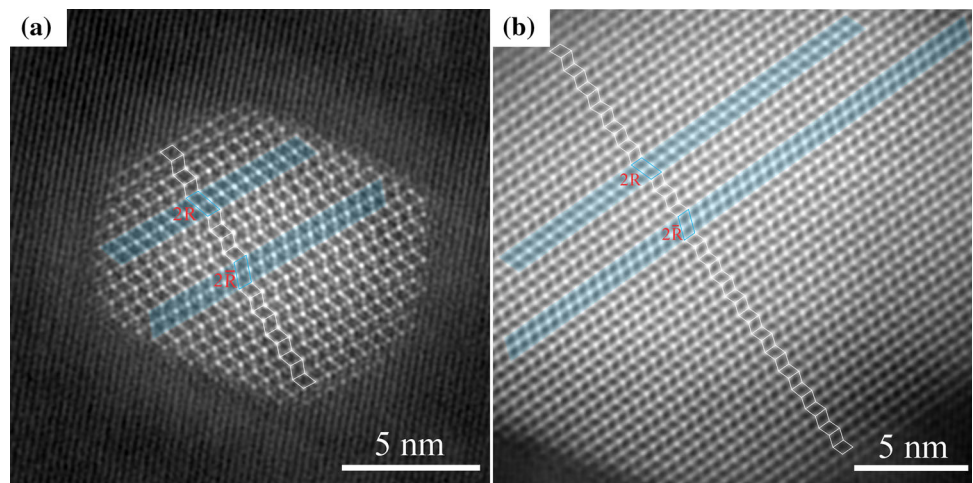
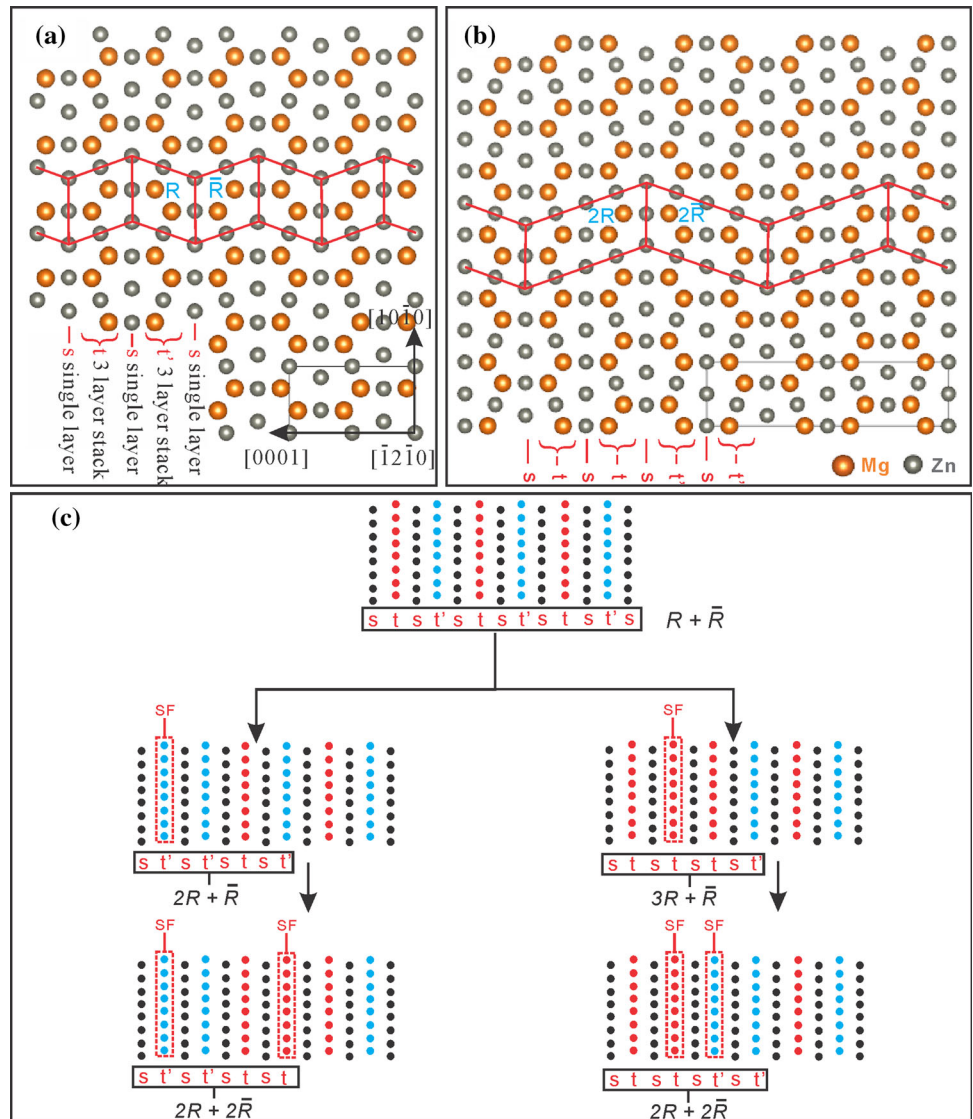


**Figure 6** Summary of the step-by-step transformations from C14 to C36 Laves structures of the MgZn<sub>2</sub> precipitate during over-aging. **a, b** Crystal models of C14-MgZn<sub>2</sub> and C36-MgZn<sub>2</sub> structures, viewed along  $[\bar{1}2\bar{1}0]$  zone axis. **c** Schematic illustration of the mechanism of C14 to C36 transformation.



dislocations gliding on the  $(0001)_n$  plane. Shockley partials can be emitted on either atomic layers  $t$  or  $t'$  and then reverse them to each other [35]. Therefore, there are two possible slip paths from C14 to C36: when the slip of the partial begins from the  $t$  stacking plane ( $t$  turns to  $t'$ ), it will result in a new stacking sequence of  $\dots s' t' s' t' s' t' s' t' \dots$  and then  $2R$  stacking faults will form (Fig. 4b), while the slip of the partial is on  $t$  stacking plane ( $t'$  turns to  $t$ ), the stacking sequence turns to  $\dots s t s t s t s t \dots$  and a  $3R$  stacking fault will occur (Fig. 4c). Both transition paths are evidenced by the HAADF-STEM image in Fig. 4a, where the  $3R + \bar{R}$  and  $2R + \bar{R}$  structures can appear at the same time in one single precipitate. Further, as the aging time increases, more Shockley partials can be emitted on some specific  $t$  or  $t'$  layers; then, the

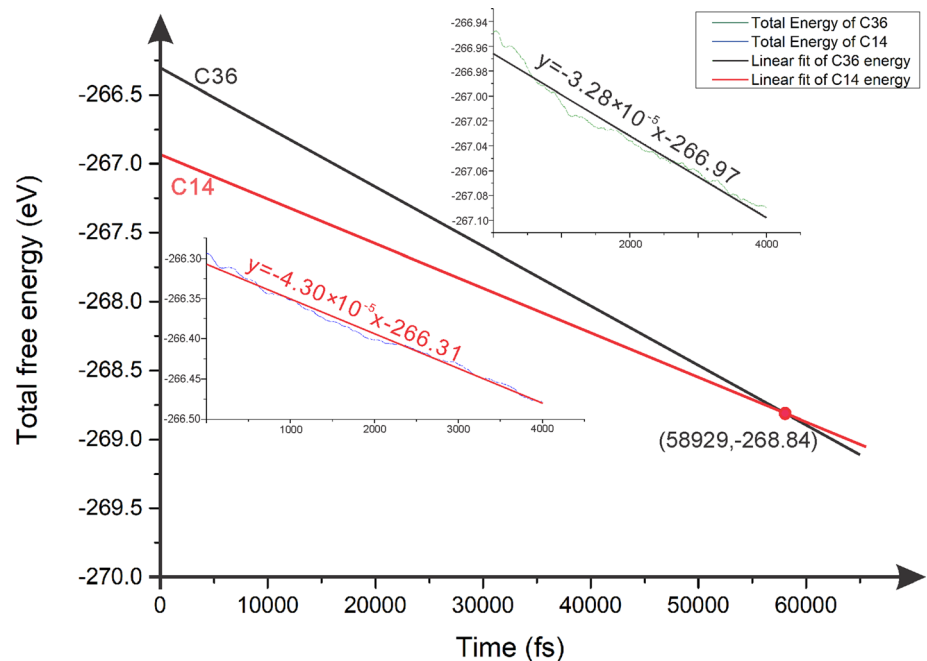
final stacking sequence of  $\dots s t s t s t' s t' \dots$  will ultimately form and a bulk C36-type Lave phase will be generated.

**Predicted energies of C14 and C36 structures**

The total free energy (taking the kinetic energy of the ions and the energy of the Nosé thermostat into account) of C14 and C36 structures at 393 K was calculated by AIMD, shown in blue and green curves. The linear fits of each total free energy curve by the Least Square Method are also displayed, marked by red and black lines, and the slopes of each line are  $-4.30 \times 10^{-5}$  eV/fs and  $-3.28 \times 10^{-5}$  eV/fs, respectively. These two fitted lines are extended to 60,000 fs in Fig. 7, and there is an intersection point at the



**Figure 7** Total free energies of C14 and C36 structures at 393 K predicted by AIMD calculations.



58929th step. Therefore, the total free energy of C36 is referred to be lower than that of C14 after a long time calculation, which can explain that why C36 precipitates only appear in the samples after an extremely long-time aging. This is consistent with our previous MD calculations [13] that the bulk free energy can be decreased when  $2R$  and  $2\bar{R}$  stacking faults (producing C36 structures) occurred in pairs inside the C14-MgZn<sub>2</sub> precipitate. Meanwhile, the average total energies of each structure are also displayed in Supplementary Document Fig. S4.

Our findings are of significance for understanding the Laves phase transformation conditions and designing materials with different types of Laves phase intermetallics. The C14 to C36 transformation is bound to influence the mechanical properties of materials, although both phases have hexagonal structures and very similar basal slip behaviors. The non-basal slip behaviors of C14 and C36 phases are different; Luo et al. [36] concluded non-basal plane slip systems in Laves phase by micro-pillar compression tests, including pyramidal slip  $\{1011\} \langle 1012 \rangle$  for C14 and  $\{1012\} \langle 1011 \rangle$  for C36. The slip behaviors have a significant impact on the properties of the alloy because the change of dislocation behavior plays a decisive role in the brittle-to-ductile transition [37]. In the current work, the effect of crystal structures on mechanical properties for Laves phases can be only studied in an indirect way,

designing an alloy with more C36-type precipitates than C14 type is scheduled.

## Conclusion

In summary, we investigated the atomic-scale transformation of MgZn<sub>2</sub> Laves phase precipitates from C14 to C36 structures by low-voltage HAADF-STEM in an Al-Zn-Mg alloy. For the first time, we report the existence of bulk C36-type MgZn<sub>2</sub> precipitates rather than C36 stacking faults, and we found the energy of C36 structure is inferred to be lower than C14 structure by AIMD calculations, in an extremely over aged state at 120 °C. Two C14-C36 transformation paths through the emission of Shockley partials on gliding planes (0001) were proposed, and atomic-scale evidence was found for the intermediate states. Our findings imply that the prototype Laves compounds will change their characteristic structures, depending on their thermal history. This important phase transformation can serve as a new strategy to control the structures of Laves phase strengthening materials and to obtain new combinations of properties.

## Acknowledgements

The basic STEM supports from Shaanxi Normal University are acknowledged.

## Funding

This work was funded by National Natural Science Foundation of China (Grant Nos. 52071340, 51820105001, and 51771234) and Youth Innovation Promotion Association CAS (Grant No. 2021192).

## Data availability

The raw data and supplementary data for these findings are available to download from the link [<https://data.mendeley.com/datasets/y8hb8vhcf8/dr aft?a=0a8906e6-2b52-49e5-824c-0f8e24c3a745>].

## Declarations

**Conflict of interest** The authors declare that they have no conflict of interest.

**Supplementary Information:** The online version contains supplementary material available at <http://doi.org/10.1007/s10853-021-06711-6>.

## References

- Stein F, Palm M, Sauthoff G (2004) Structure and stability of Laves phases. Part I. Critical assessment of factors controlling Laves phase stability. *Intermetallics*, 12:713–720
- Xie HB, Pan HC, Ren Y, Wang L, He Y, Qi X, Qin G (2018) New structured laves phase in the Mg-In-Ca system with nontranslational symmetry and two unit cells. *Phys Rev Lett* 120:085701
- Shevchenko EV, Talapin DV, Kotov NA, O'Brien S, Murray CB (2006) Structural diversity in binary nanoparticle superlattices. *Nature* 439:55–59
- Stein F, Leineweber A (2020) Laves phases: a review of their functional and structural applications and an improved fundamental understanding of stability and properties. *J Mater Sci* 56:5321–5427
- Kang LM, Yang C, Wang F, Qu SG, Li XQ, Zhang WW (2019) Deformation induced precipitation of MgZn<sub>2</sub>-type laves phase in Ti-Fe-Co alloy. *J Alloys Compd* 778:795–802
- Kang LM, Yang C, Wang F, Li XX, Zhu DZ, Zhang WW, Chen WP, Huan Y (2017) Designing ultrafine lamellar eutectic structure in bimodal titanium alloys by semi-solid sintering. *J Alloys Compd* 702:51–59
- Hazzledine PM, Pirouz P (1993) Synchroshear transformations in Laves phases. *Scr Metall Mater* 28:1277–1282
- Liu CZ, Li GP, Yuan FS, Han FZ, Zhang YD, Gu HF (2018) Stacking faults in Zr(Fe, Cr)<sub>2</sub> laves structured secondary phase particle in Zircaloy-4 alloy. *Nanoscale* 10:2249–2254
- Marioara CD, Lefebvre W, Andersen SJ, Friis J (2013) Atomic structure of hardening precipitates in an Al-Mg-Zn-Cu alloy determined by HAADF-STEM and first-principles calculations: relation to η-MgZn<sub>2</sub>. *J Mater Sci* 48:3638–3651. <https://doi.org/10.1007/s10853-013-7158-3>
- Guénolé JL, Mouhib FZ, Huber L, Grabowski B, Korte-Kerzel S (2019) Basal slip in Laves phases: the synchroshear dislocation. *Scr Mater* 166:134–138
- Huot EAJ, Ishido Y (1995) Crystal structure of multiphase alloys (Zr, Ti)(Mn, V)<sub>2</sub>. *J Alloys Compd* 231:85–89
- Murashkina TL, Syrtanov MS, Laptev RS, Stepanova EN, Lider AM (2019) Structure and defects evolution at temperature and activation treatments of the TiCr<sub>2</sub> intermetallic compound of Laves phase C36-type. *Int J Hydrogen Energy* 44:10732–10743
- Yang T, Kong Y, Lu J, Zhang Z, Yang M, Yan N, Li K, Du Y (2021) Self-accommodated defect structures modifying the growth of Laves phase. *J Mater Sci Technol* 62:203–213
- Livingston JD (1992) Laves-Phase Superalloys? *Phys Stat Sol* 131:415–423
- Emdadi A, Sizova I, Bambach M, Hecht U (2019) Hot deformation behavior of a spark plasma sintered Fe-25Al-1.5Ta alloy with strengthening Laves phase. *Intermetallics* 109:123–134
- Y. Xue, S. Li, Y. Wu, C. Liu, H. Liu, L. Yuan, Strengthening and toughening effects in laves phase Cr<sub>2</sub>Ta/Cr in-situ composites by Si additions, *Vacuum*, 174 (2020).
- Liang D, Wei C, Ren F (2021) Introducing Laves phase strengthening into an ultrafine-grained equiatomic CrFeNi alloy by niobium addition. *Mater Sci Eng A* 806
- Chung TF, Yang YL, Shiojiri M, Hsiao CN, Li WC, Tsao CS, Shi ZS, Lin JG, Yang JR (2019) An atomic scale structural investigation of nanometre-sized η precipitates in the 7050 aluminium alloy. *Acta Mater* 174:351–368
- Dumont M, Lefebvre W, Doisneau-Cottignies B, Deschamps A (2005) Characterisation of the composition and volume fraction of η' and η precipitates in an Al-Zn-Mg alloy by a combination of atom probe, small-angle X-ray scattering and transmission electron microscopy. *Acta Mater* 53:2881–2892
- Bendo A, Matsuda K, Lervik A, Tsuru T, Nishimura K, Nunomura N, Holmestad R, Marioara CD, Shimizu K, Toda H, Yamaguchi M (2019) An unreported precipitate orientation relationship in Al-Zn-Mg based alloys. *Mater Char* 158:109958.
- Bendo A, Maeda T, Matsuda K, Lervik A, Holmestad R, Marioara CD, Nishimura K, Nunomura N, Toda H, Yamaguchi M, Ikeda K-I, Homma T (2019) Characterisation of

- structural similarities of precipitates in Mg-Zn and Al-Zn-Mg alloys systems. *Philos Mag* 99:2619–2635
- [22] Rabadia CD, Liu YJ, Chen LY, Jawed SF, Wang LQ, Sun H, Zhang LC (2019) Deformation and strength characteristics of Laves phases in titanium alloys. *Mater Des*, 179
- [23] Tan L, Yang Y (2015) Microstructure and mechanical properties of laves phase-strengthened Fe-Cr-Zr alloys. *Metall Mater Trans A* 46:1188–1195
- [24] Chen H, Lu J, Kong Y, Li K, Yang T, Meingast A, Yang M, Lu Q, Du Y (2020) Atomic scale investigation of the crystal structure and interfaces of the B' precipitate in Al-Mg-Si alloys. *Acta Mater* 185:193–203
- [25] Car R, Parrinello M (1985) Unified approach for molecular dynamics and density-functional theory. *Phys Rev Lett* 55:2471–2474
- [26] Guo F, Holec D, Wang J, Li S, Du Y (2020) Impact of V, Hf and Si on oxidation processes in Ti-Al-N: insights from ab initio molecular dynamics. *Surf Coat Technol*, 381
- [27] Nose S (1991) Constant temperature molecular dynamics methods. *Prog Theor Phys* 103:1–46
- [28] Komura Y, Tokunaga K (1980) Structural studies of stacking variants in Mg-base friauf-laves phases. *Acta Cryst B* 36:1548–1554.
- [29] CT K (2002) Determination of core structure periodicity and point defect density along dislocations [PhD thesis], Arizona State University
- [30] Saito T, Ehlers FJH, Lefebvre W, Hernandez-Maldonado D, Børge R, Marioara CD, Andersen SJ, Holmestad R (2014) HAADF-STEM and DFT investigations of the Zn-containing  $\beta''$  phase in Al-Mg-Si alloys. *Acta Mater* 78:245–253
- [31] Cao FH, Zheng JX, Jiang Y, Chen B, Wang YR, Hu T (2019) Experimental and DFT characterization of  $\eta'$  nano-phase and its interfaces in Al Zn Mg Cu alloys. *Acta Mater* 164:207–219
- [32] Biskupek J, Jinschek JR, Wiedwald U, Bendele M, Han L, Ziemann P, Kaiser U (2010) Identification of magnetic properties of few nm sized FePt crystalline particles by characterizing the intrinsic atom order using aberration corrected S/TEM. *Ultramicroscopy* 110:820–825
- [33] Weng Y, Jia Z, Ding L, Du K, Duan H, Liu Q, Wu X (2018) Special segregation of Cu on the habit plane of lath-like  $\beta'$  and QP2 precipitates in Al-Mg-Si-Cu alloys. *Scr Mater* 151:33–37
- [34] Chung TF, Yang YL, Huang BM, Shi ZS, Lin JG, Ohmura T, Yang JR (2018) Transmission electron microscopy investigation of separated nucleation and in-situ nucleation in AA7050 aluminium alloy. *Acta Mater* 149:377–387
- [35] Chisholm MF, Kumar S, Hazzledine P (2005) Dislocations in complex materials. *Science* 307:701–703
- [36] Luo W, Kirchlechner C, Zavašnik J, Lu W, Dehm G, Stein F (2020) Crystal structure and composition dependence of mechanical properties of single-crystalline NbCo<sub>2</sub> Laves phase. *Acta Mater* 184:151–163
- [37] Zhang Y, Zhang W, Du B, Li W, Sheng L, Ye H, Du K (2020) Shuffle and glide mechanisms of prismatic dislocations in a hexagonal C14-type Laves-phase intermetallic compound. *Phys Rev B* 102:134117

**Publisher's Note** Springer Nature remains neutral with regard to jurisdictional claims in published maps and institutional affiliations.